A Spatial Whole-Cell Model for HBV Viral Infection and Drug Interactions

Zhaleh Ghaemi[1,2]* and Martin Gruebele[1,2,3,4,5]

[1]*Department of Chemistry, University of Illinois at Urbana-Champaign, Urbana, IL 61801, USA*
[2]*Beckman Institute, University of Illinois at Urbana-Champaign, Urbana, IL 61801, USA*
[3]*Carle-Illinois College of Medicine, University of Illinois at Urbana-Champaign, Urbana, IL 61801, USA*
[4]*Center for Biophysics and Quantitative Biology, University of Illinois at Urbana-Champaign, Urbana, IL 61801, USA*
[5]*Department of Physics, University of Illinois at Urbana-Champaign, Urbana, IL 61801, USA*

*Corresponding author: ghaemi@illinois.edu

Abstract
Despite a vaccine, hepatitis B remains a world-wide source of infections and deaths, and tackling the infection requires a multimodal approach against the virus. We develop a whole-cell model combining spatial and kinetic models for the infection cycle of a hepatocyte by hepatitis B virus (HBV). We simulate a near complete viral infection cycle with this whole cell model stochastically for 10 minutes of biological time, as a starting point to map out virus-host interaction. We find that with an established infection, decreasing the copy number of envelope proteins can shift the dominant infection pathways to amplification, resulting in higher cccDNA copy number, which may be a mode of action for siRNA drugs. Capsid mutants when destabilized such that they disassemble at nuclear pore complexes lead to increase in cccDNA copy number, but a cytoplasmic disassembly does not increase cccDNA copy number. Finally, our simulations can predict the best drug dosage and timing of administration. Our adaptable computational platform can be utilized to study other viruses and host-virus interactions.

Introduction

Whole-cell modeling is a novel approach that aims to simulate the cell cycle and to predict the cell state.[1] Whole cell models can be used to either model all essential processes within the cell, or to predict the outcome of specific processes within a realistic cellular environment.[1,2] Whole-cell models can be predictive when subjected to changes in cell environment, mutations, added drugs, and other perturbations that affect multiple networks in the cell in a highly inter-dependent manner, revealing unexpected side-effects in addition to on-target effects of applied perturbations. They provide a platform for next-generation drug development that can replace in-cell and potentially even animal studies with less costly and more ethical simulations not subject to stringent regulatory demands at early stages of the discovery process. Because of the biological relevance of the spatial arrangement of human cells, one of the key ingredients of whole-cell models is spatial degrees of freedom.[2]

Here we lay the foundation of a whole-cell model for predicting viral infection outcomes and modeling the effect of different drugs on viral replication in a realistic intracellular environment. We focus on hepatitis B virus (HBV) that chronically infects 250 million people globally.[3] Chronic hepatitis B, for which there is no cure, can lead to cirrhosis, liver failure, and is the primary cause of hepatocellular carcinoma.[3] Therefore, there is an unmet medical need to investigate HBV life

cycle steps with incompletely understood mechanisms that are related in complex ways through interaction with the cellular machinery.

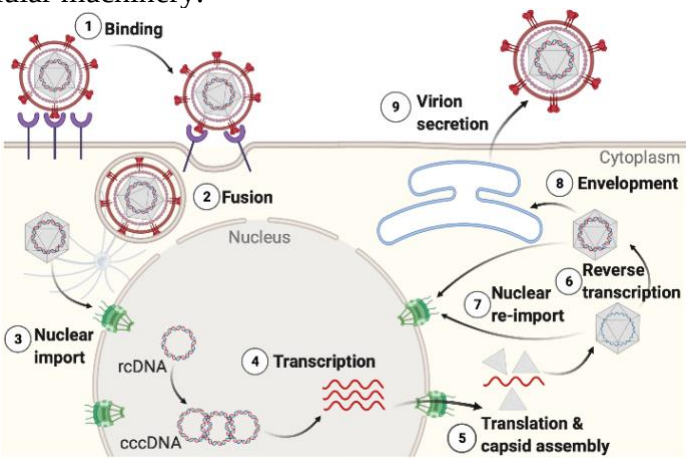

Fig. 1. The HBV life cycle. The virion binds to a host cell and the genome-containing capsid (hexagon) is released. The capsid is transported to the nucleus to replicate. New capsids are assembled and upon maturation, secreted from the host cell (secretion pathway) or re-imported back to the nucleus for further cccDNA amplification (amplification pathway).

Like other viruses, HBV exploits the internal machinery of its host cell to replicate. Upon binding to its target, the virus enters the cell in an endosomal vesicle that further releases the capsid into the cytoplasm (Figure 1). The capsid possibly travels along microtubules to reach the nucleus, where its viral genomic content, a relaxed circular DNA (rcDNA), is delivered, possibly by disassembly of the capsid at nuclear pore complexes (NPCs). Inside the nucleus, rcDNA is converted to the covalently closed circular DNA (cccDNA), which is then transcribed to multiple mRNA species, one of which translates to the core (capsid) protein, the viral pregenomic RNA (pgRNA), and the viral reverse transcriptase (RT). PgRNA, RT, and core proteins assemble to form an immature capsid. Conversion of pgRNA to rcDNA within the capsid by RT leads to capsid maturation. Through a mechanism that likely involves interaction with viral envelope proteins, the mature capsid either re-enters the nucleus for further amplification of cccDNA or is secreted from the cell after acquiring an envelope composed of viral envelope proteins embedded in the host cell lipid membrane.[4] Additionally, binding of core proteins alone leads to the formation of empty capsids, that can either be directed to the nucleus or be secreted from the cell.

The HBV life cycle has been modeled previously by mathematical and computational approaches. Murray and Goyal[5] developed an agent-based stochastic HBV infection model that could examine the effect of variable cccDNA count coupled with hepatocyte proliferation on clearance. Fatehi *et al.*[6] improved upon the previous model with a more comprehensive reaction network for infection that was solved stochastically. Their results uncovered the presence of several phases during infection. Cangelosi *et al.* developed a model that takes into account the sinusoid architecture of the liver, which the virus may exploit to become chronic.[7]

Despite the sophistication of these models, the spatial organization inside cells is still missing, basically assuming that the interior of a host hepatocyte is well-mixed. Organelles such as the nucleus and its NPCs, and diffusive or directed transport of mature or immature capsids within the host are not treated, or lumped into a single reaction rate.[6] This rate, which depends on the interaction of virus components such as cccDNA, RNA, and core proteins, has been shown to be crucial for the infection outcome, which highlights the importance of spatial resolution in a cell model of infection.[6] Additionally, we have recently shown that other processes such as RNA splicing can be significantly affected by spatial organization within the human cells.[2]

Here we combine a reaction network describing the HBV infection with a realistic spatial model of a hepatocyte, building a whole-cell model for infection whose response to initial conditions (e.g. cccDNA counts) and perturbations (e.g. drugs) can be studied to yield a more complete picture of the virus-cell interaction. We took a data-driven approach to develop the model, by integrating multiple available experimental results to mimic a realistic cellular environment. We then developed a kinetic model that describes the viral infection cycle and complemented it with a diffusion model describing how various species diffuse in different regions of the modeled cell. Both kinetic and diffusion models were parametrized with experimentally-determined values. Finally, we performed reaction-diffusion master equation simulations on the entire HBV life cycle within the *in-silico* hepatocyte for 10 minutes of biological time to explore two key questions as our first application of the model: How does the expression of viral envelope proteins into the ER membrane affect the decision process for mature virions being released vs. mature capsids being reimported to the nucleus to further amplify cccDNA? And what is the optimum dosage and timing the model predicts for HBV capsid inhibitor drugs?

The whole cell model is scalable to include more processes in the future (e.g. directed transport on microtubules, excretion of mature virions from the cell surface), and to implement experimental parameters for increased accuracy as they become known. The development of this platform could thus help virologists and others interested in HBV infection to better design experiments by testing hypotheses with the model. Such a virtuous cycle of whole cell model and experiment could lead to a comprehensive understanding of the 'hotspots' in viral infection that need to be treated by a multimodal approach.

Results

Spatially-resolved model of a hepatocyte

Following our previous data-driven strategy,[2] we constructed a spatial model of a hepatocyte. Briefly, we gathered data for each organelle from a variety of experimental studies such as cryo-electron tomography, live cell fluorescent imaging, and mass spectroscopy. The data then is interpreted to obtain the size, morphology, and number of copies of each organelle. We used set operations and custom-designed codes to faithfully represent the morphology of organelles.

Hepatocytes are epithelial cells that are polyhedral-shaped with off-centered nuclei. Therefore, our hepatocyte model has a dimension of 12.3 **μ**m × 12.3 **μ**m × 16 **μ**m,[8] as shown in Figure 2A, B. The cell organelles that were included in this model are the essential components that are involved in the viral infection process. These organelles include: the plasma membrane, the cytoplasm, the endoplasmic reticulum (ER), the microtubules organizing center (MTOC), the microtubules (MT), the mitochondria, the Golgi apparatus, the nucleus. The nucleus itself is composed of, the nuclear envelope, the nuclear pore complexes (NPCs), the nucleoplasm, the nucleolus, the Cajal bodies, and the nuclear speckles. The two latter components are liquid organelles[9].

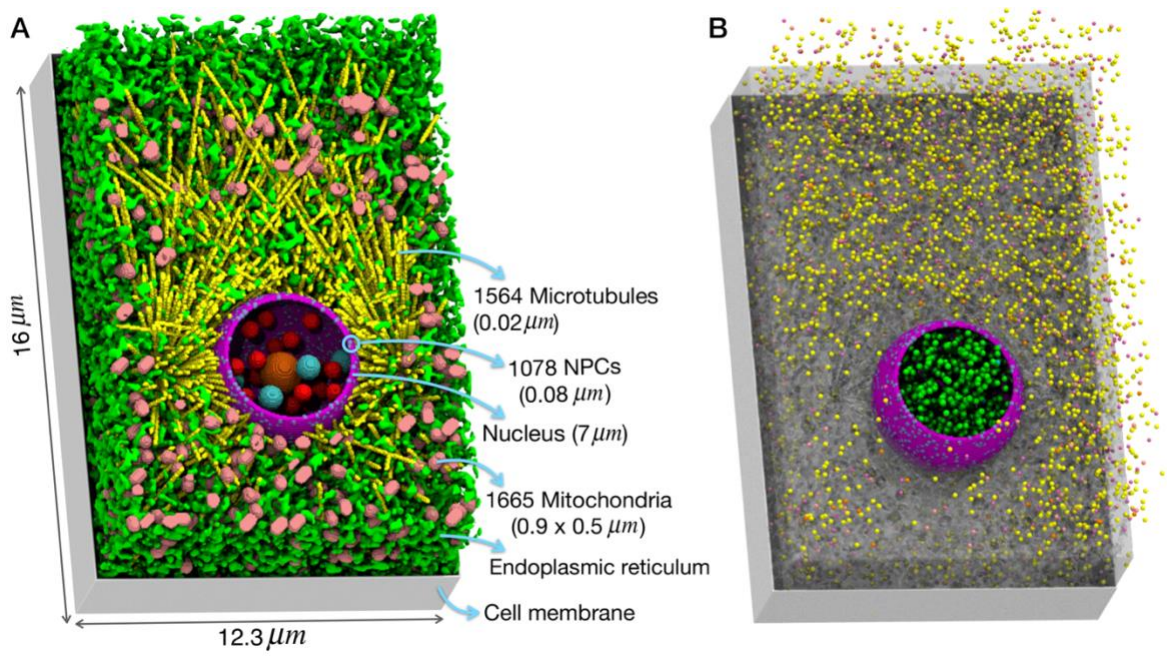

Fig. 2. A) The spatial model of the hepatocyte with 13 different organelles and compartments. B) Capsids, shown as yellow (empty), pink (RNA-containing), and orange (mature) are distributed randomly in the cytoplasm, represented as a shaded grey region. Inside the nucleus, RNA polymerase II are shown as green dots.

Similar to our previous HeLa cell model we used to study spliceosomal dynamics, the ER units were modeled using the cellular automata algorithm, starting from the nuclear envelope to the plasma membrane, and occupying about 7% of the cell volume[10]. MTOC were modeled as 4 sphero-cylindrical organelles each with the dimension of 0.5 **μ**m × 0.2 **μ**m surrounding the nucleus [11–13], from which 1564 MTs with the diameter of 0.064 nm are originated[14–16]. MTs with random orientation start from the MTOCs and end up close to the cell membrane. MTs can be involved in the transport of viruses in the cytoplasm[17]. 1665 sphero-cylindrically-shaped mitochondria with a dimension of 0.9 **μ**m × 0.5 **μ**m were randomly distributed in the cytoplasm[13,18]. A Golgi apparatus composed of five stacked sheets, each with a thickness of 0.128 **μ**m, was placed close to the nucleus.

The nuclear diameter is 7 **μ**m[19], with its envelope covered with 2660 randomly distributed NPCs[20], each with a dimension of 0.08 **μ**m[21], controlling the traffic of macromolecules between the nucleus and the cytoplasm. The nucleus contains a 0.9 **μ**m-wide nucleolus[22], and two distinct liquid organelles: nuclear speckles and Cajal bodies that are both spherically-shaped with radii of 0.35 **μ**m and 0.5 **μ**m, respectively.[9,23] Hepatocyte organelles are listed in Table 1 along with their dimensions.

Table 1. Organelles, dimensions and their counts in the model hepatocyte

Component	Dimension (**μ**m)	Number
Hepatocyte cell size	16 × 12.3 × 12.3	1
Nucleus	R = 7	1
mitochondria	0.9 × 0.5	1665
MTOC	0.5 × 0.2	4

MT	0.02	1564
ER	–	6% cell volume
NPCs	0.08	1078
Nucleolus	R = 0.9	1
Nuclear speckles	R = 0.35	20
Cajal bodies	R = 0.5	4

Kinetic model for the HBV infection

To predict the HBV infection in hepatocytes, we developed a reaction network that can faithfully represent the processes involved in infection. The processes were classified as reactions and diffusion. Because of the small counts of most involved chemical species, we considered the biological events as stochastic processes. Therefore, we use a reaction-diffusion master equation as the theoretical framework that describes the time evolution of the infection (see Methods for details). One of the most important novel aspects of our model is augmenting the reactions to a realistic cellular environment. The spatial degrees of freedom have been shown to be a crucial aspect for infection initiation in a host cell. The following biological events were modeled:

0. The viral capsid diffuses in the cytoplasm until reaching an NPC
1. DNA containing and empty capsids starts to dissociate at NPCs but the RNA-containing capsids diffuses back to the cytoplasm
2. The released relaxed circular DNA (rcDNA) molecules from the DNA-containing capsid diffuse to the nucleus until it converts to covalently-closed circular DNA (cccDNA)
3. The cccDNA is transcribed to produce viral messenger RNAs and pgRNA
4. The viral RNA transcripts pass through the NPCs and are translated in the cytoplasm to produce viral proteins
5. Viral core proteins assemble to form either empty or (pgRNA) genome-containing capsids
6. The RNA-containing capsid matures
7. Capsids bind to large (L) envelope proteins with correct stoichiometry for envelopment

Table 2. Summary of reactions describing the infection cycle

Reaction	Rate	Unit	Compartment
Capsid disassembly at NPCs			
$capsid_{DNA} \rightarrow rcDNA$	0.00167	s^{-1}	P
$capsid_{empty} \rightarrow 0$	0.00167	s^{-1}	P
rcDNA repair and transcription at nucleus			
rcDNA → cccDNA			N
cccDNA + RNA_pol → cccDNA.RNApol	0.33×10^{6}	$M^{-1}\ s^{-1}$	N
$cccDNA.RNA_{pol} \rightarrow cccDNA + RNA_pol$	10^{-3}	s^{-1}	N
$cccDNA.RNA_{pol} \rightarrow cccDNA + RNA_{pol} + pgRNA$	0.02	s^{-1}	N
$cccDNA.RNA_{pol} \rightarrow cccDNA + RNA_{pol} + LSmRNA$	0.0208	s^{-1}	N
$cccDNA.RNA_{pol} \rightarrow cccDNA + RNA_{pol} + SmRNA$	0.0238	s^{-1}	N
$cccDNA.RNA_{pol} \rightarrow cccDNA + RNA_{pol} + XmRNA$	0.0714	s^{-1}	N

cccDNA.RNA$_{pol}$ → cccDNA +RNA$_{pol}$+ preCmRNA	0.0784	s^{-1}	N
Viral proteins translation and assembly of capsids			
pgRNA → dimer + pgRNA	0.0131	s^{-1}	C
pgRNA → viral_pol + pgRNA	0.0131	s^{-1}	C
LSmRNA → L + LSmRNA	0.0139	s^{-1}	C
SmRNA → M + SmRNA	0.0156	s^{-1}	C
SmRNA → S + SmRNA	0.0156	s^{-1}	C
XmRNA → X+ XmRNA	0.048	s^{-1}	C
preCmRNA → preCmRNA + preC	0.0526	s^{-1}	C
pgRNA + viral_pol → RNP	0.33×10^{6}	M^{-1} s^{-1}	C
RNP→ pgRNA + viral_pol	10^{-3}	s^{-1}	C
RNP→ capsid$_{RNA}$	0.0003	s^{-1}	C
interm + interm → capsid$_{empty}$	0.00167	s^{-1}	C
Dimer → 0	1	s^{-1}	C
reverse transcription of the viral RNA and maturation of capsid			
capsid$_{RNA}$ → capsid$_{DNA}$	ln(2)/12*3600	s^{-1}	N
Capsid envelopment			
capsid_DNA + L → capsid_DNA.L (repeated 20 times)	$2.55\text{x}10^{7}$	M^{-1} s^{-1}	E
capsid_DNA.L → capsid_DNA + L (repeated 20 times)	0.041	s^{-1}	E
capsid_empty + L → capsid_empty.L (repeated 20 times)	$2.55\text{x}10^{7}$	M^{-1} s^{-1}	E
capsid_empty.L → capsid_empty + L	0.041	s^{-1}	E
capsid_RNA + L → capsid_RNA.L (repeated 20 times)	0.0315	M^{-1} s^{-1}	E
capsid_RNA.L → capsid_RNA + L	0.041	s^{-1}	E

The parameters describing the reactions were determined based on available experimental data or modeled based on theoretical approximations. Figure 3 shows our kinetic model to describe the infection life cycle. The reactions together with their associated rates are summarized in Table 2 (see Methods for details).

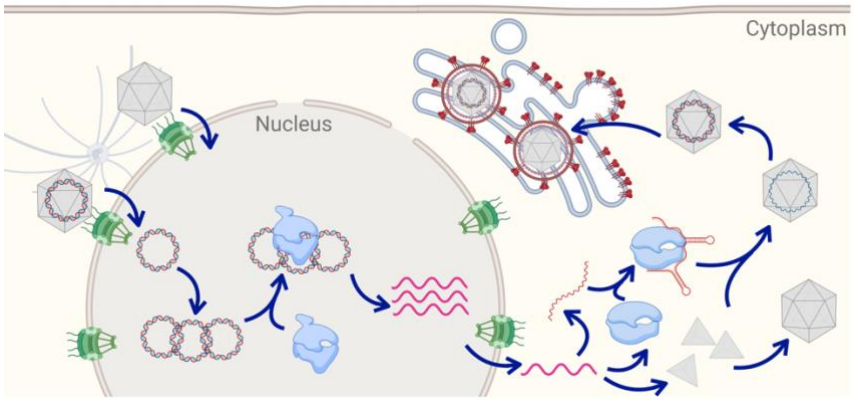

Fig. 3. The developed kinetic model describing the HBV infection cycle. The reactions and rates are listed in Table 2.

Cells switch from the secretion to the amplification pathway in response to envelope protein concentration change

It has been reported that at the start of the infection the amplification pathway is more active, namely capsids are more frequently re-imported to the nucleus, resulting in the enhancement of cccDNA production in the nucleus. In contrast, after the progression of infection, capsids are more frequently enveloped and secreted from the host cell and the secretion pathway becomes more active.[24]

In addition to the cccDNA copy number variation during the infection, one of the factors that is speculated to affect this pathway switching is the envelope protein copy number, and in particular, large (L) envelope protein that initiates the envelopment. However, whether in a cell containing an established infection (e.g., with 5 cccDNA, 52 mature capsids, 520 empty capsids[25]) varying L abundance can shift the pathways is not known. This scenario can model the effects of administering the cell with short interfering RNA (siRNA) drugs, which is known to reduce the number of L proteins. siRNA degrade target viral RNAs, thus preventing their translation.

Starting from a value of 5×10^5 copies of L[6] we simulated a near-complete infection cycle of HBV incorporated in the entire spatial model of hepatocyte for 10 minutes of biological time with varying L abundance (see Methods for details). We monitored different viral species in time to monitor how infection is evolving. Most importantly we tracked the hallmark of chronic infection, i.e., cccDNA molecules inside the nucleus at the end of our simulations. As we decrease the L abundance, the cccDNA copy number increases, indicating that more capsids are re-imported to the nucleus, disassembled at NPCs to release their viral DNA into the nucleus, and hence, the amplification pathway activates as shown in Fig. 4A. In contrast, for high L abundance the counts of cccDNA remains close to its starting value, indicating that the secretion pathway is more active. Therefore, the reduction in L counts (or increase in siRNA dosage), results in switching between pathways from secretion to amplification.

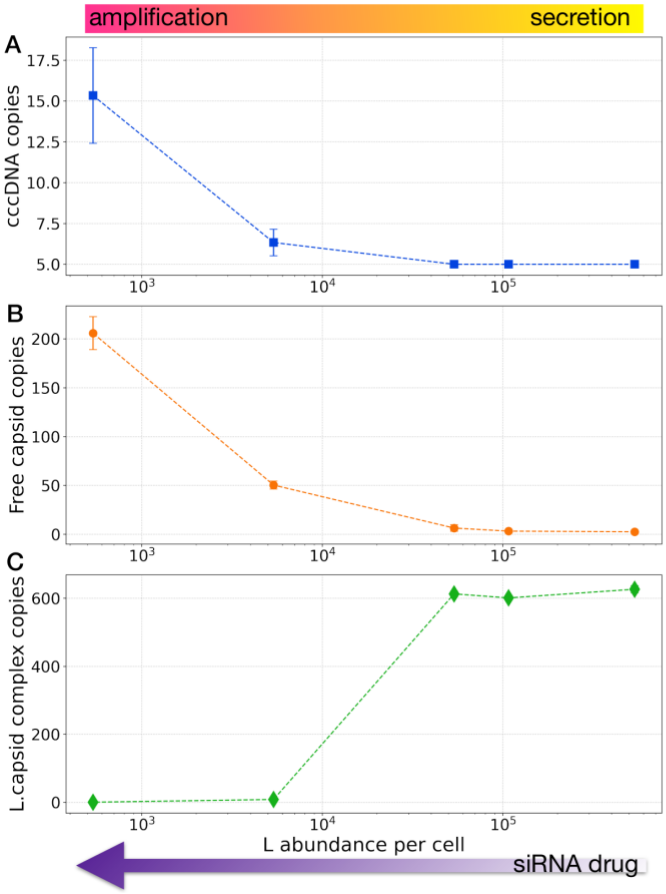

Fig. 4. Envelope protein (L) or as a proxy, administration of siRNA drugs, can switch the dominant infection pathway from secretion to amplification resulting in A) increase in cccDNA copy number, B) available capsids (both mature and empty), and C) capsid in complex with L proteins.

As the active pathway switches to amplification, capsids (mature and empty) are less frequently secreted, and therefore the number of cytoplasmic capsids is increased (Fig. 4B). Consistently, the number of the L proteins bound to the capsid (L.capsid complex), which are ready to continue with the rest of envelopment process and ultimately secretion, decreases (Fig. 4C).

These results relate L and cccDNA concentration quantitatively and demonstrate that our whole-cell model is responsive to perturbations, and capable of reproducing expected behavior. More interestingly, they show that the class siRNA drugs could lead to a contained, but increased infection within the host cell because L downregulation leads to more viral DNA in the nucleus Thus, administration of siRNA against protein L translation likely needs to be combined with other drugs, or its modification to effectively target more viral RNAs, are necessary.

Different capsid disassembly mechanisms lead to differential infection outcome

We have shown that mutations at specific regions of the core (capsid) protein can increase the level of cccDNA production with respect to the wild type capsids[26,27]. Additionally, core protein mutations can destabilize the capsid, thus enhancing its disassembly.[28]

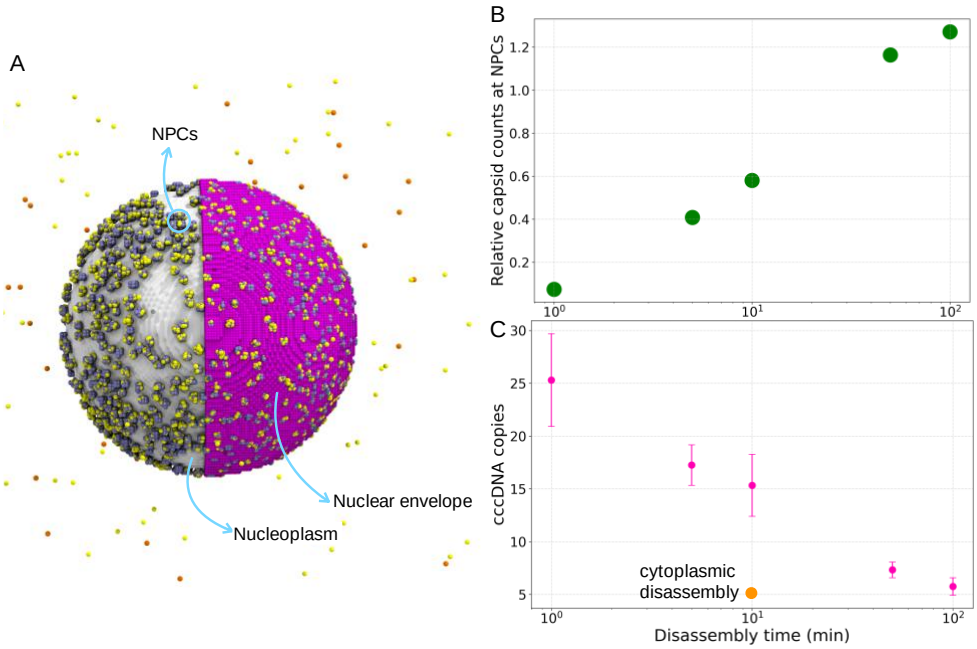

Fig. 5. Effect of capsid stability on interaction with NPCs and cccDNA count. (A) Snapshot of capsids (shown in yellow and orange) in cytoplasm and bound to nuclear pore complexes. Half the nuclear envelope is shown in purple. B) By decreasing the disassembly time: B) the relative number of capsids in NPCs decreases, and C) the number of cccDNA molecules increases provided that the mutant capsids remain stable enough not to crack in the cytoplasm.

We hypothesize that capsid mutants that increase cccDNA production destabilize the capsid only enough to accelerate its disassembly at NPCs but prevents its cracking in the cytoplasm. To test this hypothesis, we simulated the effects of the capsid mutants by varying the capsid disassembly time, from its value determined by *in vitro* time-resolved small angle X-ray scattering experiments[29] of ~ 10 minutes to the range from 1 to 100 minutes, but still occurring at NPCs. These simulations again incorporate the entire infection cycle in the realistic model of a hepatocyte. Fig. 5A shows that as the simulation progresses the capsids (orange and yellow dots) bind more to the NPCs. By decreasing the disassembly time, the normalized counts of capsids at NPCs (i.e. the ratio of the total number of capsids bound to NPCs at the end of the simulation to the same quantity after 30 s of simulation time), decreases (Fig. 5B). This result indicates that due to the faster disassembly of the mutated capsids, fewer capsids remain bound to NPCs. Following the accelerated disassembly for mutant capsids, the number of synthesized cccDNA molecules increases, which leads to enhanced infection (Fig. 5C). If on the other hand, the capsid is hyper-destabilized and the disassembly occurs in the cytoplasm (Fig. 5C, orange dot), no cccDNA is replicated beyond its initial value (5), which is an ideal mechanism for drug action, which we discuss next.

Simulations predict an effective drug dosage and the best timing for drug administration

HBV capsid inhibitor drugs (e.g. JNJ_827, or JNJ_890) can accelerate capsid assembly and by destabilizing the capsid, can lead to its enhanced disassembly.[30] Although this class of drugs can block infection, their detailed mechanism of action, and in particular their effects on the cccDNA copies, remains elusive. Therefore, we modeled the drug acting on the cell, using our whole-cell computational platform.

We assume that the drug destabilizes the capsid such that it dissociates in the cytoplasm. To determine an effective dosage of the drug, we also varied the number of capsids that are drug bound. Fig. 6A shows that 20% drug-bound capsids, are not enough to significantly reduce the cccDNA copy number. Drug dosage needs to be increased to at least bind to 50% of capsids, and reaching a factor of 2 reduction in cccDNA copy number when increasing the drug concentration to bind to 80% of capsids.

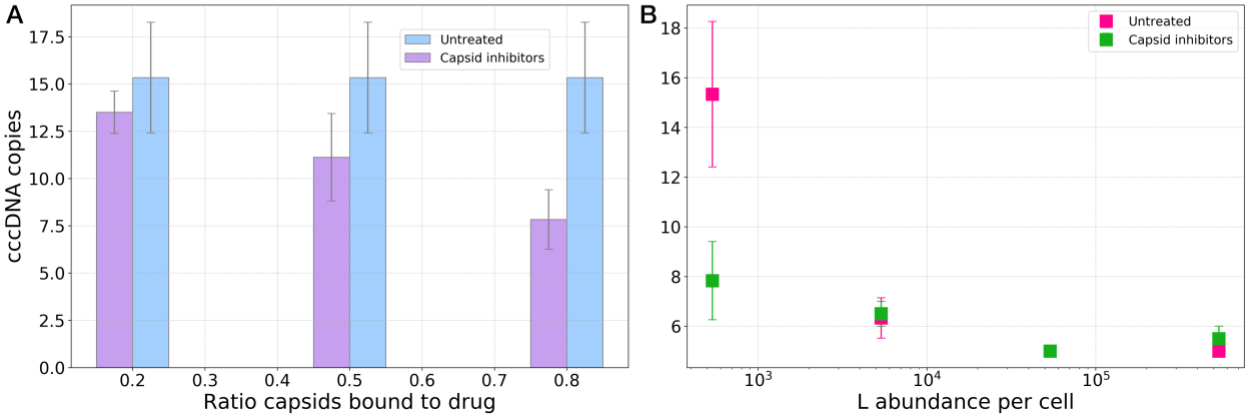

Fig. 6. Efficacy of a hypothetical drug treatment that promotes cytoplasmic dissociation of the capsid. (A) The effect of drug dosage on cccDNA copies when treated (purple) as compared to and untreated (blue, for reference) cells. (B) The timing of drug administration matters: drugs are only effective at the start of infection (or low L abundance).

Can the timing of drug administration change the effectiveness of the drug? To answer this question, we simulated the effect of drugs in different stages of infection. Specifically, we varied L abundance to produce host cells in amplification-active vs. secretion-active pathways (Fig. 4). Our results in Fig. 6B show that at the start of infection when amplification pathway is active and the protein L count is low, drug treatment effectively reduces the cccDNA copy number, which is the hallmark of infection. But as the infection progresses, and the secretion pathway becomes more active (high L counts), drugs bound to even 80% of capsids will not reduce the number of cccDNA molecules in the nucleus. This is because when secretion is dominant, capsids mostly are enveloped and secreted, leaving small number of capsids that can bind to the drugs.

Conclusions

We used a data-driven approach to construct a whole-cell computational platform for studying viral infection. Our focus in this study was on HBV, that elimination of its chronic infection is one of the goals of by the World Health Organization. We developed a spatial model for a hepatocyte (the host cell of HBV) and a kinetic model, a series of reaction that describe the viral infection. We simulated our whole-cell platform stochastically for 10 minutes of biological time. We found that, with an established infection, the decreasing the abundance of envelope (L) proteins can switch the infection pathway from dominantly secreting the capsids to re-importing them back to the nucleus, resulting in cccDNA amplification. The L protein concentration can be a proxy of siRNA drugs, indicating that this drug can lead to an increase in viral DNA. Our simulations showed the degree in which capsid mutants are destabilized can lead to a differential outcome for cccDNA copy number. Finally, by simulating the effects of capsid inhibitors, we predicted what dosage and timing of drug administration can be most effective.

Acknowledgments
M.G. was supported by the James R. Eiszner Chair. Z.G. was supported by the Department of Chemistry, as well as NSF MCB 1803786 (Gruebele).

Methods

RDME simulations methodology in LM Following detailed discussion in refs.[2,31,32] in details, we use formalism known as the reaction-diffusion master equation (RDME), which describes the state of a stochastic system to be in a specified spatial and compositional state, for the simulations in this paper. The "state" for our systems of interest, comprises of the number of each interacting species along with their positions. In RDME simulations using LM, the geometry of the system is first discretized to a cubic grid with a lattice spacing λ. Additionally, a fundamental time step τ is specified. The time evolution of the probability of the system to be in specific state **x**, containing number of molecules for each of the N_{sp} species present at each subvolume $\nu \in V$, is determined by the rates of change due to reaction and diffusion, defined by operators **R** and **D**, respectively:

$$\frac{dP(\mathbf{x},t)}{dt} = \mathbf{R}P(\mathbf{x},t) + \mathbf{D}P(\mathbf{x},t),$$

$$\frac{dP(\mathbf{x},t)}{dt} = \sum_{\nu}^{V}\sum_{r=1}^{N_{rxn}}[-a_r(\mathbf{x}_\nu)P(\mathbf{x}_\nu,t) + a_r(\mathbf{x}_\nu - \mathbf{S}_r)P(\mathbf{x}_\nu - \mathbf{S}_r,t)]$$
$$+\sum_{\nu}^{V}\sum_{\zeta}^{\pm\hat{i},\hat{j},\hat{k}}\sum_{\alpha=1}^{N_{sp}}[-d_\nu^\alpha x_\nu^\alpha P(\mathbf{x},t) + d_{\nu+\zeta}^\alpha(x_{\nu+\zeta}^\alpha + 1)P(\mathbf{x} + \mathbf{1}_{\nu+\zeta}^\alpha - \mathbf{1}_\nu^\alpha,t)]$$

The first two terms of this equation define the probability flux within each subvolume due to reactions: $a_r(\mathbf{x_\nu})$ is the reaction propensity for reaction r of N_{rxn} reactions and $\mathbf{S}r$ is the $N \times R$ stoichiometric matrix describing the net change in molecules number when a reaction occurs. The last two terms describe the rate of the change of the probability due to molecules' propensity to diffuse between neighboring subvolumes. d_ν^α is the diffusive propensity for a molecule of species α to jump to a neighboring subvolume, and is related to the macroscopic diffusion. The first part of the diffusion operator defines the probability flux out of the current state due to the diffusion of molecules from subvolume ν; and the second part of the diffusion operator, describes the diffusion of molecules into the current state from subvolumes, ν+η, where η defines the neighboring subvolume in ±*x*, ±*y*, ±*z* directions. Using an approximation for sampling the RDME equation, as implemented in LM, simulations of biologically relevant timescales (10 mins) for the hepatocyte model on multiple GPU hardware became possible.

RDME simulation details the goal of our simulations is to study how a specific infection parameter/drug affect the infection. Therefore, all our simulations started from an infected cell with an steady-state viral components that were determined previously.[6,25] All simulations started with 5 cccDNA, 52 mature capsids, 260 RNA-containing capsids, 520 empty capsids, 59 pgRNA, and 680 RNA polymerase II, and ~ 500 L proteins when its counts is not specified. Our whole-cell model contains 169 reactions occurring between 89 chemical species. All simulation time steps were 9.3 x 10^{-5} s, and lattice spacing was 64 nm. Thse chemical species counts were written every 10 time step. All simulations were performed for 10 mins of biological times on multi-GPU clusters.

References

(1) Karr, J. R.; Sanghvi, J. C.; Macklin, D. N.; Gutschow, M. V; Jacobs, J. M.; Bolival, B.; Assad-Garcia, N.; Glass, J. I.; Covert, M. W. A Whole-Cell Computational Model Predicts Phenotype from Genotype. *Cell* **2012**, *150* (2), 389–401. https://doi.org/10.1016/j.cell.2012.05.044.

(2) Ghaemi, Z.; Peterson, J. R.; Gruebele, M.; Luthey-Schulten, Z. An In-Silico Human Cell Model Reveals the Influence of Spatial Organization on RNA Splicing. *PLOS Comput. Biol.* **2020**, *16* (3), 1–23. https://doi.org/10.1371/journal.pcbi.1007717.

(3) Grimm, D.; Thimme, R.; Blum, H. E. HBV Life Cycle and Novel Drug Targets. *Hepatol. Int.* **2011**, *5* (2), 644–653. https://doi.org/10.1007/s12072-011-9261-3.

(4) Diab, A.; Foca, A.; Zoulim, F.; Durantel, D.; Andrisani, O. The Diverse Functions of the Hepatitis B Core/Capsid Protein (HBc) in the Viral Life Cycle: Implications for the Development of HBc-Targeting Antivirals. *Antiviral Res.* **2018**, *149* (October 2017), 211–220. https://doi.org/10.1016/j.antiviral.2017.11.015.

(5) Murray, J. M.; Goyal, A. In Silico Single Cell Dynamics of Hepatitis B Virus Infection and Clearance. *J. Theor. Biol.* **2015**, *366*, 91–102. https://doi.org/10.1016/j.jtbi.2014.11.020.

(6) Fatehi, F.; Bingham, R. J.; Dykeman, E. C.; Patel, N.; Stockley, P. G.; Twarock, R. An Intracellular Model of Hepatitis b Viral Infection: An in Silico Platform for Comparing Therapeutic Strategies. *Viruses* **2021**, *13* (1). https://doi.org/10.3390/v13010011.

(7) Cangelosi, Q.; Means, S. A.; Ho, H. A Multi-Scale Spatial Model of Hepatitis-B Viral Dynamics. *PLoS One* **2017**, *12* (12), 1–28. https://doi.org/10.1371/journal.pone.0188209.

(8) Wiśniewski, J. R.; Hein, M. Y.; Cox, J.; Mann, M. A "Proteomic Ruler" for Protein Copy Number and Concentration Estimation without Spike-in Standards. *Mol. Cell. Proteomics* **2014**, *13* (12), 3497–3506. https://doi.org/10.1074/mcp.M113.037309.

(9) Spector, D. L.; Lamond, A. I. Nuclear Speckles. **2011**, 1–12. https://doi.org/10.1101/cshperspect.a000646.

(10) Itzhak, D. N.; Tyanova, S.; Cox, J.; Borner, G. H. H. Global, Quantitative and Dynamic Mapping of Protein Subcellular Localization. *Elife* **2016**, *5* (JUN2016), 1–36. https://doi.org/10.7554/eLife.16950.

(11) Nigg, E. A.; Stearns, T. The Centrosome Cycle: {Centriole} Biogenesis, Duplication and Inherent Asymmetries. *Nat Cell Biol* **2011**, *13* (10), 1154–1160. https://doi.org/10.1038/ncb2345.

(12) Debec, A.; Sullivan, W.; Bettencourt-Dias, M. Centrioles: Active Players or Passengers during Mitosis? *Cell. Mol. Life Sci.* **2010**, *67* (13), 2173–2194. https://doi.org/10.1007/s00018-010-0323-9.

(13) Milo, R.; Jorgensen, P.; Moran, U.; Weber, G.; Springer, M. BioNumbers—the Database of Key Numbers in Molecular and Cell Biology. *Nucleic Acids Res.* **2009**, *38* (suppl_1), D750–D753. https://doi.org/10.1093/nar/gkp889.

(14) McEwen, B. F.; Chan, G. K. T.; Zubrowski, B.; Savoian, M. S.; Sauer, M. T.; Yen, T. J. CENP-E Is Essential for Reliable Bioriented Spindle Attachment, but Chromosome Alignment Can Be Achieved via Redundant Mechanisms in Mammalian Cells. *Mol. Biol. Cell* **2001**, *12* (9), 2776–2789. https://doi.org/10.1091/mbc.12.9.2776.

(15) Chakraborty, S.; Jasnin, M.; Baumeister, W. Three-dimensional Organization of the Cytoskeleton: A Cryo-electron Tomography Perspective. *Protein Sci.* **2020**, *29* (6), 1302–1320. https://doi.org/10.1002/pro.3858.

(16) Alushin, G. M.; Lander, G. C.; Kellogg, E. H.; Zhang, R.; Baker, D.; Nogales, E. High-Resolution Microtubule Structures Reveal the Structural Transitions in Aβ-Tubulin upon GTP Hydrolysis. *Cell* **2014**, *157* (5), 1117–1129. https://doi.org/10.1016/j.cell.2014.03.053.

(17) Blondot, M. L.; Bruss, V.; Kann, M. Intracellular Transport and Egress of Hepatitis B Virus. *J. Hepatol.* **2016**, *64* (1), S49–S59. https://doi.org/10.1016/j.jhep.2016.02.008.

(18) Weibel, E. R.; Stäubli, W.; Gnägi, H. R.; Hess, F. A. Correlated Morphometric and Biochemical Studies on the Liver Cell. *J. Cell Biol.* **1969**, *42* (1), 68–91. https://doi.org/10.1083/jcb.42.1.68.

(19) Peters, R. Nucleo-Cytoplasmic Flux and Intracellular Mobility in Single Hepatocytes Measured by Fluorescence Microphotolysis. *EMBO J.* **1984**, *3* (8), 1831–1836. https://doi.org/10.1002/j.1460-2075.1984.tb02055.x.

(20) Dultz, E.; Ellenberg, J. Live Imaging of Single Nuclear Pores Reveals Unique Assembly Kinetics and Mechanism in Interphase. *J. Cell Biol.* **2010**, *191* (1), 15–22. https://doi.org/10.1083/jcb.201007076.

(21) Mahamid, J.; Pfeffer, S.; Schaffer, M.; Villa, E.; Danev, R.; Kuhn Cuellar, L.; Forster, F.; Hyman, A. A.; Plitzko, J. M.; Baumeister, W. Visualizing the Molecular Sociology at the HeLa Cell Nuclear Periphery. *Science (80-.).* **2016**, *351* (6276), 969–972. https://doi.org/10.1126/science.aad8857.

(22) Heyden, S.; Ortiz, M. Investigation of the Influence of Viscoelasticity on Oncotripsy. *Comput. Methods Appl. Mech. Eng.* **2017**, *314*, 314–322. https://doi.org/https://doi.org/10.1016/j.cma.2016.08.026.

(23) Mirko Klingauf,* David Stanˇ ek, and K. M. N. Enhancement of U4/U6 Small Nuclear Ribonucleoprotein Particle Association in Cajal Bodies Predicted by Mathematical Modeling. *Mol. Biol. Cell* **2006**, *17*, 4972–4981. https://doi.org/10.1091/mbc.E06.

(24) Tuttleman, J. S.; Pourcel, C.; Summers, J. Formation of the Pool of Covalently Closed Circular Viral DNA in Hepadnavirus-Infected Cells. *Cell* **1986**, *47* (3), 451–460. https://doi.org/10.1016/0092-8674(86)90602-1.

(25) Balagopal, A.; Hwang, H. S.; Grudda, T.; Quinn, J.; Sterling, R. K.; Sulkowski, M. S.; Thio, C. L. Single Hepatocyte Hepatitis B Virus Transcriptional Landscape in HIV Coinfection. *J. Infect. Dis.* **2019**, *221* (9), 1462–1469. https://doi.org/10.1093/infdis/jiz607.

(26) Xi, J.; Luckenbaugh, L.; Hu, J. *Multiple Roles of PP2A Binding Motif in Hepatitis B Virus Core Linker and PP2A in Regulating Core Phosphorylation State and Viral Replication*; 2021; Vol. 17. https://doi.org/10.1371/journal.ppat.1009230.

(27) Cui, X.; Luckenbaugh, L.; Bruss, V.; Hu, J. Alteration of {Mature} {Nucleocapsid} and {Enhancement} of {Covalently} {Closed} {Circular} {DNA} {Formation} by {Hepatitis} {B} {Virus} {Core} {Mutants} {Defective} in {Complete}-{Virion} {Formation}. *J Virol* **2015**, *89* (19), 10064–10072. https://doi.org/10.1128/JVI.01481-15.

(28) Xi, J.; Cui, X.; Liu, K.; Liu, H.; Wang, J. Region-Speci Fi c Hepatitis B Virus Genome Exposure from Nucleocapsid Modulated by Capsid Linker Sequence and Inhibitor : Implications for Uncoating.

(29) Chevreuil, M.; Lecoq, L.; Wang, S.; Gargowitsch, L.; Nhiri, N.; Jacquet, E.; Zinn, T.; Fieulaine, S.; Bressanelli, S.; Tresset, G. Nonsymmetrical Dynamics of the HBV Capsid Assembly and Disassembly Evidenced by Their Transient Species. *J. Phys. Chem. B* **2020**, *124* (45), 9987–9995. https://doi.org/10.1021/acs.jpcb.0c05024.

(30) Guo, F.; Zhao, Q.; Sheraz, M.; Cheng, J.; Qi, Y.; Su, Q.; Cuconati, A.; Wei, L.; Du, Y.; Li, W.; Chang, J.; Guo, J.-T. HBV Core Protein Allosteric Modulators Differentially Alter CccDNA Biosynthesis from de

Novo Infection and Intracellular Amplification Pathways. *PLoS Pathog.* **2017**, *13* (9), e1006658. https://doi.org/10.1371/journal.ppat.1006658.

(31) Roberts, E.; Stone, J. E.; Luthey-Schulten, Z. Lattice Microbes: High-Performance Stochastic Simulation Method for the Reaction-Diffusion Master Equation. *J. Comput. Chem.* **2013**, *34* (3), 245–255. https://doi.org/10.1002/jcc.23130.

(32) Hallock, M. J.; Stone, J. E.; Roberts, E.; Fry, C.; Luthey-Schulten, Z. Simulation of Reaction Diffusion Processes over Biologically Relevant Size and Time Scales Using Multi-GPU Workstations. *Parallel Comput.* **2014**, *40* (5–6), 86–99. https://doi.org/10.1016/j.parco.2014.03.009.